Sensors and Actuators A 278 (2018) 43–47

Contents lists available at ScienceDirect

Sensors and Actuators A: Physical

journal homepage: www.elsevier.com/locate/sna

Phase derivative thermo-spatiogram for distributed temperature sensing based on chirped grating-Michelson Interferometer

Daryl Tan[a,b,c], Kok-Sing Lim[a,*], Muhammad Khairol Annuar Zaini[a], Chai-Hong Yeong[b,c], Yin-How Wong[b,c], Hang-Zhou Yang[d], Harith Ahmad[a]

[a] Photonics Research Centre, University of Malaya, 50603 Kuala Lumpur, Malaysia
[b] Dept of Biomedical Imaging, Faculty of Medicine, University of Malaya, 50603 Kuala Lumpur, Malaysia
[c] School of Medicine, Faculty of Health and Medical Sciences, Taylor's University, 47500 Subang Jaya, Selangor Darul Ehsan, Malaysia
[d] School of Physics, Northwest University, Xi'an, Shaanxi 710069, China

ARTICLE INFO

Article history:
Received 17 November 2017
Received in revised form 23 February 2018
Accepted 16 May 2018
Available online 17 May 2018

Keywords:
Thermo-spatiogram
Chirped fiber Bragg grating
Michelson interferometer

ABSTRACT

A novel thermometric measurement based on chirped fiber Bragg grating (CFBG) and Michelson Interferometer is proposed. The interrogation technique is based on the linear relation between the temperature and the phase derivative function of the grating, which is determined through Fourier transformation of the output spectrum. The Michelson interferometer configuration offers the flexibility in adjusting the position of coupling coefficient curve in the spatiogram, enabling the interrogation to be done at a shorter optical spectrum record length which can reduce the interrogation time and computation load.

1. Introduction

Fiber Bragg grating (FBG) is a mature fiber optic sensor widely used for numerous applications. In particular, the use of FBGs for distributed measurement has been reported for various applications [1,2]. In general, interferometric system and fast Fourier transform (FFT) are widely used for the characterization of the complex reflection coefficient, complex coupling coefficient and phase response of the grating [3–5]. It is commonly known that the free spectral range (FSR) of the fringes formed should be minimally two times larger than the spectral sampling resolution of the interrogator / optical spectrum analyzer so that they can be spectrally resolved [3]. This limits the suitable range of the arm lengths for the interferometer. Large sampling size may increase the accuracy of the measurement but at the expense of higher computation load and longer processing time. Hence, cost-efficient and fast interrogation technique is desired.

Inspired by the Froggatt's works [4,5], we have devised an interrogation technique for linear chirped grating in a Michelson Interferometric system to achieve distributed temperature measurement in this work. By using Fourier transform, a describing function for the coupling coefficient amplitude and phase response of the grating in the spatial domain is generated. From which a phase derivative function is formulated to describe the temperature distribution within the grating. Based on the technique, we can achieve fast optical spectral interrogation at a minimal record length without compromising the quality of the output spectrum. Furthermore, it is applicable for spectral interrogation device with medium resolution.

2. Simulation and experiment

The relation between reflection function, $r(\sigma)$ and coupling coefficient $q^*(z)$ of a grating is given by

$$r(\sigma) = -\int_0^{\infty} q^*(z) \exp\left(j2\int_0^z \sigma dz'\right) dz \quad (1)$$

where z is the local position along the grating.

The detuning coefficient, σ can be expressed as

$$\sigma = \frac{2\pi n_0}{\lambda} - \frac{\pi}{\Lambda} \quad (2)$$

* Corresponding author.
E-mail address: kslim@um.edu.my (K.-S. Lim).

https://doi.org/10.1016/j.sna.2018.05.029
0924-4247/

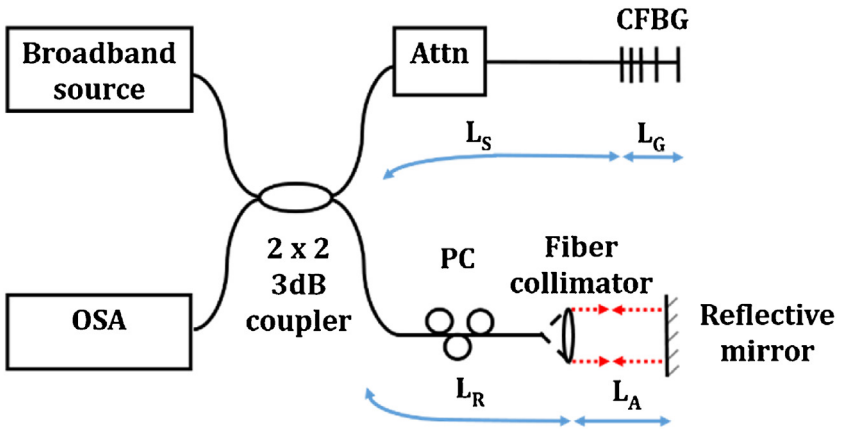

Fig. 1. Michelson interferometry setup for distributed FBG sensor. OSA: optical spectrum analyzer; Attn: fiber attenuator; PC: polarization controller. L_G: grating length, L_S: fiber length of the sensing arm (inclusive of the attenuator), L_R: fiber length of the reference arm (inclusive of the fiber collimator), L_A: air cavity length.

where n_0 is the effective index of the unperturbed fiber core, Λ is the grating period and λ is the operating wavelength. In a uniform grating, σ is independent of z, Eq. (1) can be rewritten as:

$$r(\sigma) = -\int_0^{\infty} q^*(z)\exp(j2\sigma z)\,dz \tag{3}$$

Based on the first Born approximation [6], the Fourier transform pair of (3) is given by:

$$-q^*(z) = \frac{1}{2\pi}\int_{-\infty}^{\infty} r(\sigma)\exp(-j2\sigma z)\,d\sigma \tag{4}$$

where $q^*(z)$ is the conjugate of coupling coefficient, $q(z)$.

In the context of CFBG, the detuning coefficient $\sigma_c(z)$ is a varying function of z along the grating:

$$\sigma_c(z) = \sigma + \varphi(z) = \frac{2\pi n(z)}{\lambda} - \frac{\pi}{\Lambda(z)} \tag{5}$$

The information of temperature distribution over the grating region is embedded in the effective index, $n(z)$ and grating period, $\Lambda(z)$:

$$n(z) = n_0[1 + \alpha\Delta T(z)] \tag{6.a}$$

$$\Lambda(z) = (\Lambda_0 + rz)[1 + \gamma\Delta T(z)] \tag{6.b}$$

where $\Delta T(z)$ is the profile of temperature change over the grating region, α is the thermo-optic coefficient, γ is the thermal expansion coefficient and r is the chirped rate. Based on Binomial approximation, $\varphi(z)$ can be expressed as

$$\varphi(z) \approx \frac{2\pi n_0\alpha\Delta T(z)}{\lambda} + \frac{\pi r z}{\Lambda_0^2} + \frac{\pi\gamma\Delta T(z)}{\Lambda_0} \tag{7}$$

The reflection function $r_c(\sigma)$ of a chirped grating is given by

$$r_c(\sigma) = -\int_0^{\infty} q^*(z)\exp\left\{j2\int_0^z \left[\sigma + \varphi(z')\right]dz'\right\}dz \tag{8}$$

Since σ is independent of z, (8) can be simplified as

$$r_c(\sigma) = -\int_0^{\infty} q^*(z)\exp\left[j2\int_0^z \varphi(z')dz'\right]\exp(j2\sigma z)\,dz \tag{9}$$

Analogous to (4), the Fourier transform pair of (9) is given by

$$-q^*(z)\exp\left[j2\int_0^z \varphi(z')dz'\right] = \frac{1}{2\pi}\int_{-\infty}^{\infty} r_c(\sigma)\exp(-j2\sigma z)\,d\sigma \tag{10}$$

The phase information of the CFBG can be accessed by incorporate it in a Michelson Interferometer in which the reflected beam from the CFBG (sensing arm) interferes with the reference beam from a broadband reflective mirror (reference arm) as illustrated in Fig. 1. The CFBG used here has a wide reflection band starting from 1537 nm to 1553 nm and a grating length, L_G of ~11 mm (chirp rate of 1 nm/mm). The free end of the CFBG was angled cleaved to ensure that the reflected beam from CFBG is unaffected by the Fresnel reflection from the fiber end. The reflectivity of the CFBG used in the setup is approximately 40% which is well within the acceptable range for the first Born approximation (10–50%) [7]. The other arm of the interferometer is a reference arm which comprises of polarization controller, a collimator and adjustable reflective mirror. To achieve the maximum extinction ratio in the output spectrum, a fiber attenuator based on a coiled fiber is used for lowering the high reflected intensity from the sensing arm and to match the reflected intensity from the other arm. The bending loss of the coiled fiber can be controlled by manipulating the length of the coiled fiber and the diameter of the coil. The polarization controller is used for manipulating and matching the polarization states of the beams from both arms of the interferometer. The fiber length for the sensing arm is deliberately made to be slightly longer than that of the reference arm. The optical path length difference between two arms can be compensated by the air cavity length, L_A in the reference arm which can be controlled by the moveable reflective mirror mounted on linear translation stage.

The reflection function of the Michelson interferometer can be written as

$$R(\sigma) = -\int_0^{\infty} q^*(z)\exp\left[j2\int_0^z \varphi(z')dz'\right]\exp(j2\sigma z)\,dz + a\exp\left(j2\beta d\right) \tag{11}$$

where a is a reflection coefficient of the mirror, β ($\beta = 2\pi n/\lambda$) is propagation constant of fiber, n is the effective refractive index of the fiber and d is the path difference ($d = L_S - L_R - L_A/n$). The output spectral power of the interferometer is given by $R(\sigma)R^*(\sigma)$:

$$R(\sigma)R^*(\sigma) = a^2 + \int_0^{\infty} q^*(z)\exp\left[j2\int_0^z \varphi(z')dz'\right]\exp(j2\sigma z)\,dz\int_0^{\infty} q(s)$$

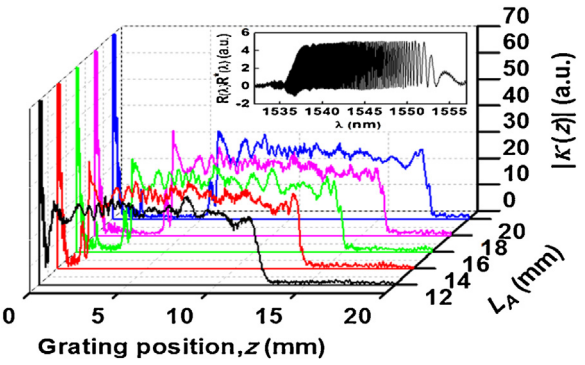

Fig. 2. Spatiogram of $|\kappa(z)|$ for different air cavity length, L_A. Inset shows the output spectrum at L_A = 14 mm (d = ~2 mm). [Ls = 104.2 cm, L_R = 103.0 cm, n = 1.448, $d\lambda$ ~25 nm and N = 2501].

$$\exp\left[-j2\int_0^s \varphi(s')ds'\right]\exp(-j2\sigma s)\,ds - a\exp(j\frac{2\pi d}{\Lambda})\int_0^{\infty} q(z)\exp\left[-j2\int_0^z \varphi(z')dz'\right]\exp[-j2\sigma(z-d)]\,dz - a\exp(-j\frac{2\pi d}{\Lambda})\int_0^{\infty} q^*(z)\exp\left[j2\int_0^z \varphi(z')dz'\right]\exp[j2\sigma(z-d)]\,dz \quad (12)$$

Spatial variables s and s' are introduced to distinguish the two independent integrals in the second term of (12). The Fourier transformation of (12) produces a describing function $K(z)$

$$F\left\{R(\sigma)R^*(\sigma)\right\} = K(z) = a^2\delta(z) - \int_{-\infty}^{\infty} q^*(s)q(z+s)\exp\left[-j2\int_0^s \varphi(z')dz'\right]\exp\left[j2\int_z^{z+s} \varphi(z')dz'\right]ds - a\exp(j\frac{2\pi d}{\Lambda})q(d-z)\exp\left[-j2\int_d^{d-z} \varphi(z')dz'\right] - a\exp(-j\frac{2\pi d}{\Lambda})q^*(d+z)\exp\left[j2\int_d^{d+z} \varphi(z')dz'\right] \quad (13)$$

The second term of (13) is an autocorrelation of the coupling coefficient with its conjugate. The integral equals to zero for z in the range of $L_G < z < S - L_G$, where S is the length of the produced spatiogram. Since the third and fourth terms of (13) are mirror pairs and they share the same phase information, the fourth term is chosen for the ensuing analysis:

$$\kappa(z) = -a\exp(-j\frac{2\pi d}{\Lambda})q^*(d+z)\exp\left[j2\int_d^{d+z} \varphi(z')dz'\right] \quad (14)$$

3. Result and discussion

Fig. 2 shows the curves of describing function $|\kappa(z)|$ for different air cavity lengths, L_A. The rectangular curve represents the magnitude of coupling coefficient of the CFBG in the spatiogram and its position can be shifted by controlling L_A. The mirror pair of this coupling coefficient can be found at the other side of the spatiogram (not shown in the graph). Inset shows the output spectrum of the interferometer at L_A = 14 mm (d = ~2 mm). The extinction ratio of the fringes was optimized by matching the polarization states (with PC) and intensities (with attenuator) of the beams from both arms of the interferometer. This enhances the accuracy of the produced describing function $|\kappa(z)|$. The varying FSR of the fringes from one edge to the other one of the grating reflection band (refer inset) can be attributed to the linearly varying path length difference between the local grating (with varying grating period along the chirped grating structure) and the mirror. The overall FSR will be larger when $|d|$ is approaching zero. The interference spectrum with large FSR is a preferred choice because they can be spectrally resolved and the measurement is more reliable.

The phase function $\phi(z)$ of $\kappa(z)$ is given by:

$$\phi(z) = arg\,[\kappa(z)] = \phi_0 + 2\int_d^{d+z} \varphi(z')dz' \quad (15)$$

where ϕ_0 is the sum of phases of all non z-dependent terms in (14).

Differentiation of (15) with respect to z yields:

$$\frac{d\phi(z)}{dz} = 2\varphi(d+z) = 2\left[\frac{2\pi n_0\alpha\Delta T(d+z)}{\lambda} + \frac{\pi r(d+z)}{\Lambda_0^2} + \frac{\pi\gamma\Delta T(d+z)}{\Lambda_0}\right] \quad (16)$$

Let κ_{Ref} (z) and ϕ_{Ref} (z) be the reference coupling coefficient and phase function in which $\Delta T(z) = 0$. The term $\pi r(d+z)/{\Lambda_0}^2$ can be eliminated by subtracting $\phi(z)$ with $\phi_{Ref}(z)$ and the following expression is formulated.

$$\Phi(z) = \frac{d}{dz}\left[\phi(z) - \phi_{\mathrm{Ref}}(z)\right] = \frac{d}{dz}\left\{arg\left[\frac{\kappa(z)}{\kappa_{\mathrm{Ref}}(z)}\right]\right\} = 2\pi\left(\frac{2n_0\alpha}{\lambda} + \frac{\gamma}{\Lambda_0}\right)\Delta T(z+d) \quad (17)$$

The spatial resolution of the spatiogram is given by [8]:

$$dz = \frac{\lambda_c^2}{2nd\lambda} \quad (18)$$

where λ_c represents central wavelength and $d\lambda$ the wavelength span of the recorded spectrum. The length of the spatiogram is defined as $S = Ndz$; where N is the sample size of the recorded spectrum. Given that $d\lambda$ ~25 nm and N = 2501, the calculated spatial resolution for the spatiogram in Fig. 2 is ~0.033 mm.

By adjusting the position of the reflective mirror (manipulating L_A) in the experimental setup, the coupling coefficient function can be shifted to the leftmost position of the spatiogram, a minimum sample size N of 1480 is sufficient to accommodate the curve of coupling coefficient function and its mirror pair in the spatiogram. This can enhance the processing speed of the interrogation. However, it is worth noting that the element of $\delta(z)$ is located at z = 0 in the spatiogram and it is important to keep a small distance between the curve of the coupling coefficient function and $\delta(z)$ to ensure the phase information of the coupling coefficient function is intact.

Fig. 3 shows the output phase shift derivative $\Phi(z)$ in response to a heat source located at different positions along the grating. The heat source is a hot wire (60 μm diameter tungsten wire) in which the induced temperature can be varied by controlling the electric current through the wire. As described in Eq. (17), the output phase shift derivative $\Phi(z)$ is linearly proportional to the local temperature change $\Delta T(d+z)$ on the grating structure. The contact point

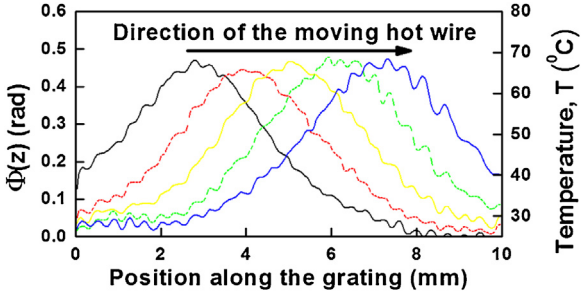

Fig. 3. Plots of phase shift derivative $\Phi(z)$ correspond to hot wire at different positions (uniform distance of ~1.2 mm) within the grating region. The secondary y-axis shows the corresponding temperature. (L_A = 14 mm, $d\lambda$ ~25 nm, N = 2501).

of the grating with the hot wire experiences the highest change in local temperature and the peak of the $\Phi(z)$ curve marks the position of the hot wire. A total of 5 output spectra were recorded at interval of 40 s to produce the 5 $\Phi(z)$ curves in Fig. 3. The y-axis represents corresponding local temperature, T on the grating. It can be observed that the peak changes its position at a uniform displacement of ~1.2 mm. This is in agreement with the hot wire moving speed of 0.03 mm/s.

Fig. 4(a) shows the temporal response of the measured temperature distribution of a moving hot wire (constant temperature ~70 °C) along the grating. The output spectrum was periodically recorded by the OSA at an interval of 10 s into a computer via a GPIB card using LabVIEW. After that, the temperature distribution profiles generated from the spectra were combined to formulate this temporal-spatiogram. During the measurement, the hot wire was mounted on a linear translation stage traveling at a constant speed of 30 μm/s from one end to the other end of the CFBG and returned. The motion and temperature distribution of the hot wire are as depicted in this temporal-spatiogram. The measured position (position of peak temperature in the spatiogram) has a good linearity of R^2 ~ 0.991 (standard deviation ~0.25 mm) with the actual position of the hot wire (Refer Fig. 4(b)). Fig. 5(a) shows the output response of the CFBG on a stationary hot wire with varying temperature. The applied current through hot wire was increased from 0 A at t = 100 s until 2.0 A at t = 500 s at a rate of 0.1 A every 20 s. The red dotted line in the graph indicates the temperature variation of the hot wire (calibrated using thermocouple). It is observed that the measured temperature (by the proposed system) is linearly proportional to the squared of the applied current, I^2 and a maximum temperature of 240 °C was recorded. We believe that maximum detected temperature can be further enhanced if the CFBG is pre-annealed at higher temperature or a regenerated CFBG is used [9]. The measured temperature plummets down to room temperature when the current is terminated (at t = 500 s). Fig. 5(b) shows the linear relationship between phase shift derivative, measured tem-

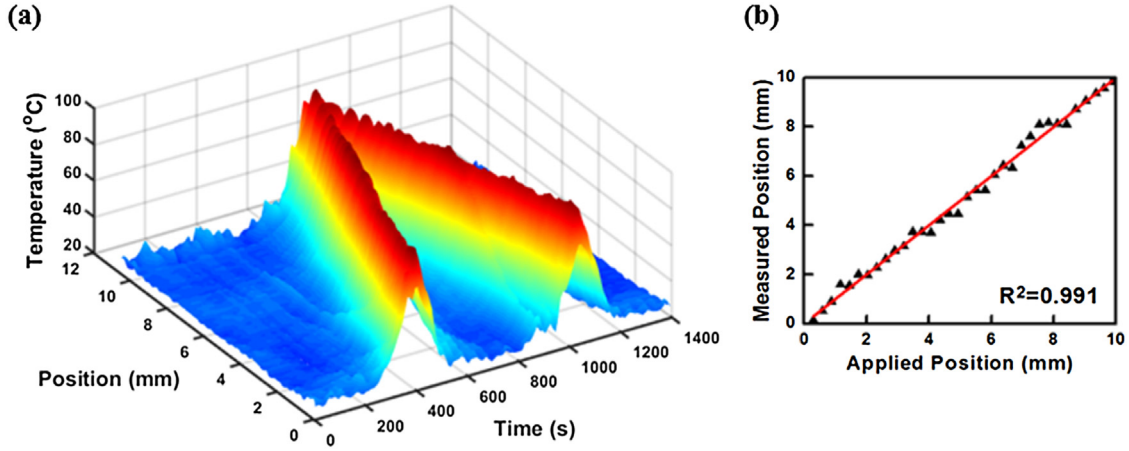

Fig. 4. (a) Measured temperature profile of a moving hot wire along the CFBG. (b) The linear correlation between measured position (by proposed sensor) with the actual position of the moving hot wire. (L_A = 14 mm, $d\lambda$ ~25 nm, N = 2501).

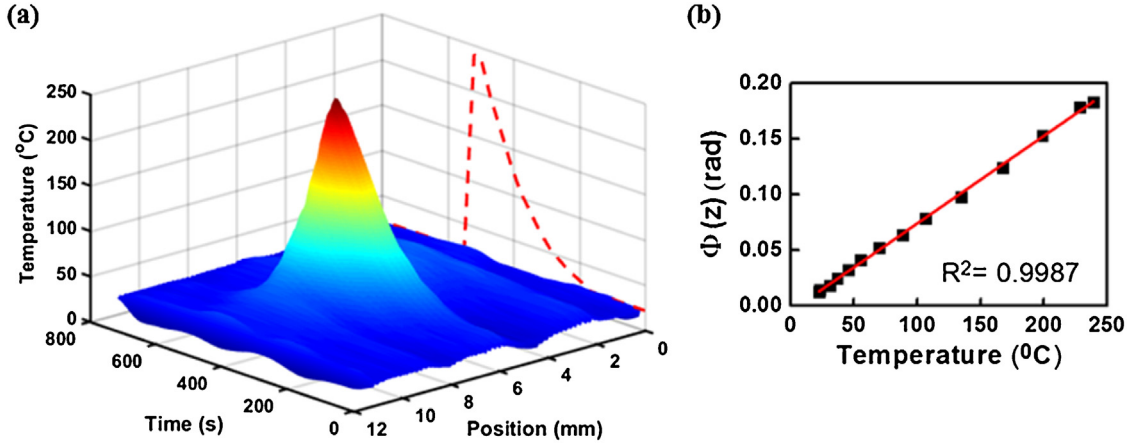

Fig. 5. (a) Temperature profile of a stationary hot wire with increasing current. Red dotted line shows the temperature variation of the hot wire (calibrated using a thermocouple). (b) The relationship between phase shift derivative, $\Phi(z)$, measured temperature and applied temperature of the hot wire. (L_A = 14 mm, $d\lambda$ ~25 nm, N = 2501) (For interpretation of the references to colour in this figure legend, the reader is referred to the web version of this article).

perature and applied temperature of the hot wire. The temperature sensitivity of the sensor is estimated to be 7.67×10^{-4} rad/°C. The measured temperature and applied temperature have a good linear correlation of $R^2 \sim 0.999$ and a standard deviation of ~1.4 °C. This measurement error can be attributed to the fluctuating temperature of hot wire due to the ambient air perturbation and noise in the recorded optical spectrum.

4. Conclusion

In overall, we have experimental demonstrated a thermo-spatiogram based on CFBG-Michelson Interferometer system. Through Fourier transform, the temperature profile within the grating can be determined from the phase derivative function. Our findings indicate that the proposed system has good linearity in both temperature and spatial measurements. Taking the example of the graph in Fig. 4(a), since the translation velocity / stage position is known, the time axis of the graph can be converted into a spatial axis, hence two-dimensional temperature mapping for any heat source is possible using this approach. The use of a moveable reflective mirror in this interferometer offers the flexibility of variable fringe FSR and position shifting of coupling coefficient curve in the spatiogram, to facilitate fast optical spectral interrogation and processing speed for the acquired spectra.

Acknowledgments

This work was supported in part by the PRGS (PR002-2017A), FRGS (FP006-2014B), National Natural Science Foundation of China (61405160), and ShaanXi Young Scientist Star Program (2016KJXX-04).

References

[1] A.M. Gillooly, L. Zhang, I. Bennion, Implementation of a distributed temperature sensor utilizing a chirped Moire fiber Bragg grating, Opt. Commun. 242 (2004) 511–242515.
[2] Y. Lu, C. Baker, L. Chen, X.Y. Bao, Group-delay-based temperature sensing in linearly-chirped fiber Bragg gratings using Kerr phase-interrogator, J. Lightw. Technol. 33 (2015) 381–385.
[3] J. Skaar, Measuring the group delay of fiber Bragg gratings by use of end-reflection interference, Opt. Lett. 24 (1999) 1020–1022.
[4] M. Froggatt, Distributed measurement of the complex modulation of a photoinduced Bragg grating in an optical fiber, Appl. Opt. 35 (1996) 5162–5164.
[5] M. Froggatt, J. Moore, Distributed measurement of static strain in an optical fiber with multiple Bragg gratings at nominally equal wavelengths, Appl. Opt. 37 (1998) 1741–1746.
[6] J. Skaar, Fiber Bragg grating sensors, in: A. Cusano, A. Cutolo, J. Albert (Eds.), Fiber Bragg Grating Sensors: Recent Advancement, Industrial Applications, and Market Exploitation, Bentham Science Publishers, 2011, pp. 39–40.
[7] H. Kogelnik, Filter response of nonuniform almost-periodic structures, Bell Sys, Tech. J. 55 (1976) 109–126.
[8] S. Kieckbusch, C. Knothe, E. Brinkmeyer, Fast and accurate characterization of fiber bragg gratings with high spatial and spectral resolution, Proc. OFC, March (2003) 379–381.
[9] X. Qiao, Y. Wang, H. Yang, T. Guo, Q. Rong, L. Li, D. Su, K. Lim, H. Ahmad, Ultrahigh-temperature chirped fiber Bragg grating through thermal activation, IEEE Photon. Technol. Lett. 27 (2015) 1305–1308.

Biographies

Daryl Tan received B.Sc. and M.Sc. in Department of Physics, Faculty of Science, University of Malaya, Malaysia in 2011 and 2016 respectively. Currently works as Ph.D student in Department of Biomedical Imaging, Faculty of Medicine, University of Malaya.

Kok-Sing Lim received the B.E. degree from the Department of Electrical Engineering, Faculty of Engineering, University of Malaya, Malaysia, in 2008, and the Ph.D. degree from the Photonics Research Centre, Department of Physics, University of Malaya, in 2012. He is currently a Senior Lecturer with the Photonics Research Centre, University of Malaya. He is a corporate member of Institute of Engineers Malaysia (IEM), a registered Professional Engineer (Telecommunication) with the Board of Engineers Malaysia (BEM) and a member of IEEE as well as OSA. His current research interests include fiber Bragg grating sensors, Spatial Division Multiplexing and medical laser devices.

Muhammad Khairol Annuar Bin Zaini received the Bachelor degree from the Department of Physics, Faculty of Science, University Putra Malaysia, Malaysia, in 2015, and currently a postgraduate candidate at Photonics Research Centre, University of Malaya. His current research interest include fiber Bragg grating sensors, and Spatial Division Multiplexing technology.

Chai-Hong Yeong is a medical physicist and senior lecturer at the Department of Biomedical Imaging, Faculty of Medicine, University of Malaya, Kuala Lumpur, Malaysia. Dr. Yeong obtained her PhD with Distinction from the University of Malaya in 2012. She is the current Secretary General of Medical Physics Subgroup in Malaysia, as well as a member of the American Association of Physicists in Medicine (AAPM) and the International Organization of Medical Physics (IOMP). She is also one of the founding committee of the ASEAN College of Medical Physics (ACOMP), established in Nov 2014. Dr. Yeong has published extensively in several academic journals, proceedings, academic book and book chapters. Her research areas focus on theranostics (therapy + diagnostic), targeted radionuclide therapy, shear wave elastography, image-guided minimally invasive cancer therapy, as well as oral drug delivery using biomedical imaging techniques. Her researches have won several local and international awards including the Certificate of Merit awarded by the European Society of Radiology, 2012.

Hang-Zhou Yang received the B.Eng. degree in telecommunication engineering from Air Force Engineering University, China, in 2005, and the Ph.D. degree in photonic research from the University of Malaya, in 2012. He is currently an Assistant Professor at College of Physics, Northwest University, China. His current research interests include fiber optic sensing and communication technologies, and micro and nanophotonics.

Harith Ahmad received the Ph.D. degree in laser technology from the University of Wales Swansea, U.K., in 1983. He is currently a Distinguished Professor with the Department of Physics, University of Malaya. He is the Director of the Photonics Research Centre with the University of Malaya, Kuala Lumpur, Malaysia. He is a Fellow of the Malaysian Academic of Science.